I&EC research
Industrial & Engineering Chemistry Research

ARTICLE

pubs.acs.org/IECR

Synthesis of Dimethyl Carbonate from Carbon Dioxide and Methanol over $Ce_xZr_{1-x}O_2$ and [EMIM]Br/$Ce_{0.5}Zr_{0.5}O_2$

Zhi-Fang Zhang,[†,§] Zhong-Wen Liu,[†,‡] Jian Lu,[†] and Zhao-Tie Liu*[,†,‡]

[†]Key Laboratory of Applied Surface and Colloid Chemistry (Shaanxi Normal University), Ministry of Education, Xi'an 710062, China
[‡]School of Chemistry and Materials Science, Shaanxi Normal University, Xi'an 710062, China
[§]School of Chemistry and Chemical Engineering, Yulin University, Yulin 719000, China

ABSTRACT: The solid solution series $Ce_xZr_{1-x}O_2$ (x = 0.2, 0.3, 0.4, 0.5, 0.6, 0.8, 1.0) with a bimodal pore structure was prepared by the citric acid sol−gel method. Results from X-ray diffraction, Raman spectroscopy, scanning electron microscopy, mercury porosimetry, and N_2 adsorption/desorption measurements indicated that the physical properties of the solid solutions were significantly affected by the Ce/Zr molar ratio and the calcination temperatures. These solid solutions can be used in the synthesis of dimethyl carbonate (DMC) from methanol and carbon dioxide. Results indicated that the structure of the solid solutions and the Ce/Zr molar ratio in $Ce_xZr_{1-x}O_2$ were the key factor in determining the catalytic activity for the synthesis of DMC. Higher catalytic performance was observed with a 1:1 Ce/Zr molar ratio at a calcination temperature of 1273 K. 1,1,1-Trimethoxymethane (TMM) was used to remove residual H_2O in situ, and was found to increase the methanol conversion from 1.8 to 7.9% at 373 K under a pressure of 20 MPa after 24 h. The combination of the bimodal porous catalyst with an effective H_2O removal agent gave a methanol conversion of 10.4% at 373 K, under 12 MPa after 34 h. The catalytic activity was almost doubled when the ionic liquid 1-ethyl-3-methylimidazolium bromide was loaded on $Ce_{0.5}Zr_{0.5}O_2$, which may be a promising means for selective production of DMC from CO_2 and CH_3OH.

INTRODUCTION

Dimethyl carbonate (DMC) has many potential applications as an environmentally benign chemical product. It is achieving increasing importance in the chemical industry because it can be used as both a reagent and a solvent, and has found application in carbonylation and methylation reactions.[1,2] DMC is also attractive because of its low impact on human health and the environment.[3,4] It is also potentially a gasoline fuel additive, with three times the oxygen content of the commonly used methyl tert-butyl ether (MTBE).[5]

Several reaction routes have been reported for the synthesis of DMC.[6] Among these methods, the direct synthesis of DMC from carbon dioxide (CO_2) and methanol (CH_3OH) (eq 1) is the preferred route because it adheres to "green" chemistry principles.[7−11] Moreover, conversion of CO_2 into useful industrial compounds has attracted much attention[12] as it is environmentally benign (i.e., nontoxic, noncorrosive, and nonflammable). The activation of CO_2 is the key problem in its conversion to DMC.[13]

$$2CH_3OH + CO_2 \rightarrow (CH_3O)_2CO + H_2O \qquad (1)$$

A number of effective catalysts have been reported for promoting the reaction of CH_3OH with CO_2 to form DMC. Among the catalysts investigated, including organometallic compounds,[14] carbonate salts,[15] and oxides,[16−18] $Ce_xZr_{1-x}O_2$ solid solutions showed potential for higher catalytic performance.[19−21] It is believed that these solid solutions have both acidic and basic sites,[22] which are both important for the selective synthesis of DMC from CH_3OH and CO_2.[19,23] However, the methanol conversion rates remain low due to the thermodynamic limitation of the reaction, even in the presence of dehydrating agents such as $CaCl_2$,[24] 2.2-dimethoxy propane (DMP),[16] acetals,[25,26] and molecular sieves.[27] Catalyst deactivation and hydrolysis of the DMC caused by the coproduced water were postulated to be the reasons for the low yield.[25] Moreover, both the catalytic activity and selectivity for DMC are strongly influenced by the crystal size and surface properties of the solid solution, which in turn depend on the preparation methods and calcination conditions of the catalyst. Enhancing the conversion of methanol and selectivity for DMC remain major challenges. Other approaches to solving these problems, such as removing H_2O,[25] modifying the catalyst,[28] and adding coreagents[15] have been reported.

In this work, a series of $Ce_xZr_{1-x}O_2$ (x = 0.2, 0.3, 0.4, 0.5, 0.6, 0.8, 1.0) solid solutions with a bimodal pore structure were synthesized. The catalytic performances of $Ce_xZr_{1-x}O_2$ and the ionic liquid 1-ethyl-3-methylimidazolium bromide loaded on $Ce_{0.5}Zr_{0.5}O_2$ ([EMIM]Br/$Ce_{0.5}Zr_{0.5}O_2$) were investigated for the title reaction. To overcome the thermodynamic limitations of the title reaction, 1,1,1-trimethoxymethane (TMM) was also added to remove water (eq 2).

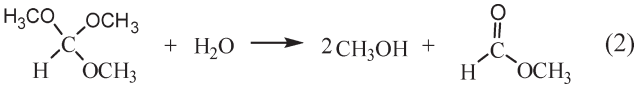

(2)

EXPERIMENTAL SECTION

Catalyst Preparation. $Ce_xZr_{1-x}O_2$ catalysts were synthesized with different Ce/Zr molar ratios (x = 0.2, 0.3, 0.4, 0.5, 0.6, 0.8, and 1.0) via a citric acid sol−gel process using $Ce(NO_3)_3 \cdot 6H_2O$

Received: October 5, 2010
Accepted: January 2, 2011
Revised: December 31, 2010
Published: January 19, 2011

dx.doi.org/10.1021/ie102017j | Ind. Eng. Chem. Res. 2011, 50, 1981–1988

and $Zr(NO_3)_4 \cdot 4H_2O$ as precursors. First, solutions of $Ce(NO_3)_3 \cdot 6H_2O$ and $Zr(NO_3)_4 \cdot 4H_2O$ in ethanol (0.2 mol·L^{-1}, molar ratio of Ce^{3+}/Zr^{4+} = 1.0, 100 mL each) were poured into a 400-mL beaker. A solution of citric acid in ethanol (0.2 mol·L^{-1}, 100 mL) was then slowly added with stirring. The mixture was stirred for a further 24 h at room temperature, and then a citric acid sol−gel was obtained after the solvent was evaporated at 353 K. After drying in air at 353 K for 24 h, the citric acid sol−gel changed into a xerogel. The xerogel was then calcined at 773 (designated as CZO), 923, 1073, 1173, or 1273 K (designated as $Ce_{0.5}Zr_{0.5}O_2$) in air for 4 h. The material was heated at 1 K·min^{-1} from room temperature to 373 K, held at 373 K for 60 min, then heated at a rate of 3 K·min^{-1} from 373 to 773 K, held at 773 K for 60 min, and then heated at a rate of 5 K·min^{-1} from 773 to 923 K (or 1073, 1173, or 1273 K).

[EMIM]Br/$Ce_{0.5}Zr_{0.5}O_2$ was prepared by adding the appropriate amount of $Ce_{0.5}Zr_{0.5}O_2$ to a solution of [EMIM]Br in methanol. The mixture was stirred for 6 h and then the solvent was evaporated at 313 K. Finally, the material was dried at 333 K overnight.

Catalyst Characterization. X-ray diffraction (XRD) studies were carried out on a D/Max 2550VB+/PC (Rigaku, Japan) X-ray diffractometer with Cu Kα radiation (λ = 1.5406 Å) and a Ni filter. The X-ray tube was operated at 30 kV and 20 mA. Samples were scanned from 2θ of 20 to 80° and the XRD line positions were determined with a step size of 0.02° and a counting time of 2.5 s per step. The morphologies were studied by SEM analysis on a Quanta 200 apparatus, Philips-FEI Co. (30 kV high vacuum modes, resolution: 3.5 nm, Holland).

Pore size distributions (PSD) were determined by the mercury porosimetry method with a PoreMaster/PoreMaster GT. POREMASTER - (33/60). Moving point avg. Eleven (Scan Mode), frequency 50 Hz, power (max) 1000 VA (excluding vacuum pump).

Textural properties were determined by N_2 adsorption/desorption at 77 K using automatic Micromeritics ASAP 2020 equipment. Data were treated in accordance with the BET and BJH methods from the desorption branch (17−3000 Å). The solid solutions were degassed at 623 K for at least 6 h to remove any adsorbed impurities before isotherms were recorded.

CO_2 pulse chemisorption was performed on a Micromeritics AutoChem II 2920 instrument equipped with a thermal conductivity detector (TCD). First, the samples (about 200 mg) were pretreated in a quartz U-tube in a helium stream at 773 K. The samples were then cooled to room temperature under He at a flow rate of 50 cm^3 min^{-1} before being exposed to 10 pulses of the corresponding probe molecule. The amount of gas desorbed was determined by time integration of the TPD-curves.

The reduction behavior of the samples was examined by temperature programmed reduction (TPR) on a Micromeritics AutoChem II 2920 instrument. All of the experiments used 5% H_2 in argon with a flow rate of 50 cm^3 min^{-1}. The temperature was increased from room temperature to 1073 K at a rate of 10 K·min^{-1}. The water produced by reduction was trapped into a cold trap. The consumption of H_2 was quantitatively measured by time integration of the TPR-profiles.

Synthesis of DMC from CO_2 and CH_3OH. The direct synthesis of DMC from CO_2 and CH_3OH was carried out in a stainless-steel autoclave reactor with an inner volume of 100 mL. Eight g of CH_3OH or a mixture of CH_3OH and TMM (A. R. grade, Xi'an Chemical Industries) and 0.5 g of catalyst were put into the autoclave, and then the reactor was purged with carbon dioxide. The mixture was heated and magnetically stirred after adjusting the autoclave to the desired pressure with CO_2, which is under subcritical or supercritical condition. The reaction was carried out over a range of temperatures and pressures (6, 12, 16, and 20 MPa).

Products in either the liquid or gas phases were analyzed by gas chromatography (GC, SP6800, Shandong Lu'nan Co. equipped with FID and TCD detectors). An HP-5 capillary column was used to separate the liquid products from the unconverted CH_3OH, and a packed column of GDX-102 was used to separate the gaseous products.

RESULTS AND DISCUSSION

XRD and Raman Characterization. The crystal and surface structure of the CZO and $Ce_{0.5}Zr_{0.5}O_2$ catalysts were characterized by XRD and Raman shifts. Figure 1a and b are the XRD patterns and Raman shift spectra, respectively, for CZO, and Figure 1c and d are those for $Ce_{0.5}Zr_{0.5}O_2$.

The XRD patterns of CZO (Figure 1a) showed that there was no diffraction peak from either CeO_2 or ZrO_2, indicating that CZO was formed via homogeneous mixing of Ce and Zr ions. However, it is difficult to determine the phases of nanocrystalline $Ce_xZr_{1-x}O_2$ based on the XRD data alone.[29,30] As reported in a recent paper,[31] the crystal structure of $Ce_xZr_{1-x}O_2$ can be differentiated through the combination of XRD and Raman spectroscopy.

The combined data from XRD and Raman measurements (Figure 1b) revealed that the samples consisted mainly of the tetragonal phase (t) for the CZO samples for x = 0.2−0.3, mainly the monoclinic phase of ZrO_2 at x = 0.4, and mainly the cubic phase (c) for x = 0.5−1.0. These results indicated that the phase composition on the surface was directly related to the Ce/Zr molar ratio in the CZO solid solutions. The crystal size of CZO was calculated using the Debye−Scherrer formula based on the diffraction peak at a 2θ of about 29.20°, as shown in Table 1, indicating the nanocrystalline nature of the calcined powders.

The crystal structure of $Ce_{0.5}Zr_{0.5}O_2$ was also determined from a combination of XRD (Figure 1c) and Raman data (Figure 1d). $Ce_{0.5}Zr_{0.5}O_2$, was mainly the c phase for the $Ce_{0.5}Zr_{0.5}O_2$ sample calcined at 773 K, and the amount of t phase in the sample increased as the calcination temperature increased, with the $Ce_{0.5}Zr_{0.5}O_2$ sample calcined at 1273 K being predominately t phase. Based on the Debye−Scherrer formula and the diffractions at about 29.3° shown in Figure 1c, the average grain sizes of the $Ce_{0.5}Zr_{0.5}O_2$ samples calcined at 773, 1073, and 1273 K were calculated to be 19.5, 19.6, and 23.5 nm, respectively. This gradual increase in the crystal size of $Ce_{0.5}Zr_{0.5}O_2$ may be caused by stronger sintering at higher temperatures. The catalytic activity is not only related to the total size of sample, but also the size of active site and type of active site.

Morphology and Physical Properties. The morphologies of the CZO samples were observed by SEM (Figure 2), and the mesopore size distributions were determined by the BJH method from the desorption branch (17−3000 Å) of the N_2 adsorption−desorption isotherm at 77 K (Table 2).

Figure 2 shows the SEM micrographs of the CZO samples. Macropores with a worm-hole like shape gradually became uniform as the Ce molar ratio increased from 0.2 to 0.8 (Figure 2a−f). The pore diameter varied from about 1 to 4 μm as the molar ratio of Ce/Zr in CZO changed.

Table 2 shows the pore size distributions (PSD), BET surface areas, and pore volumes of the CZO samples. The mesoporous

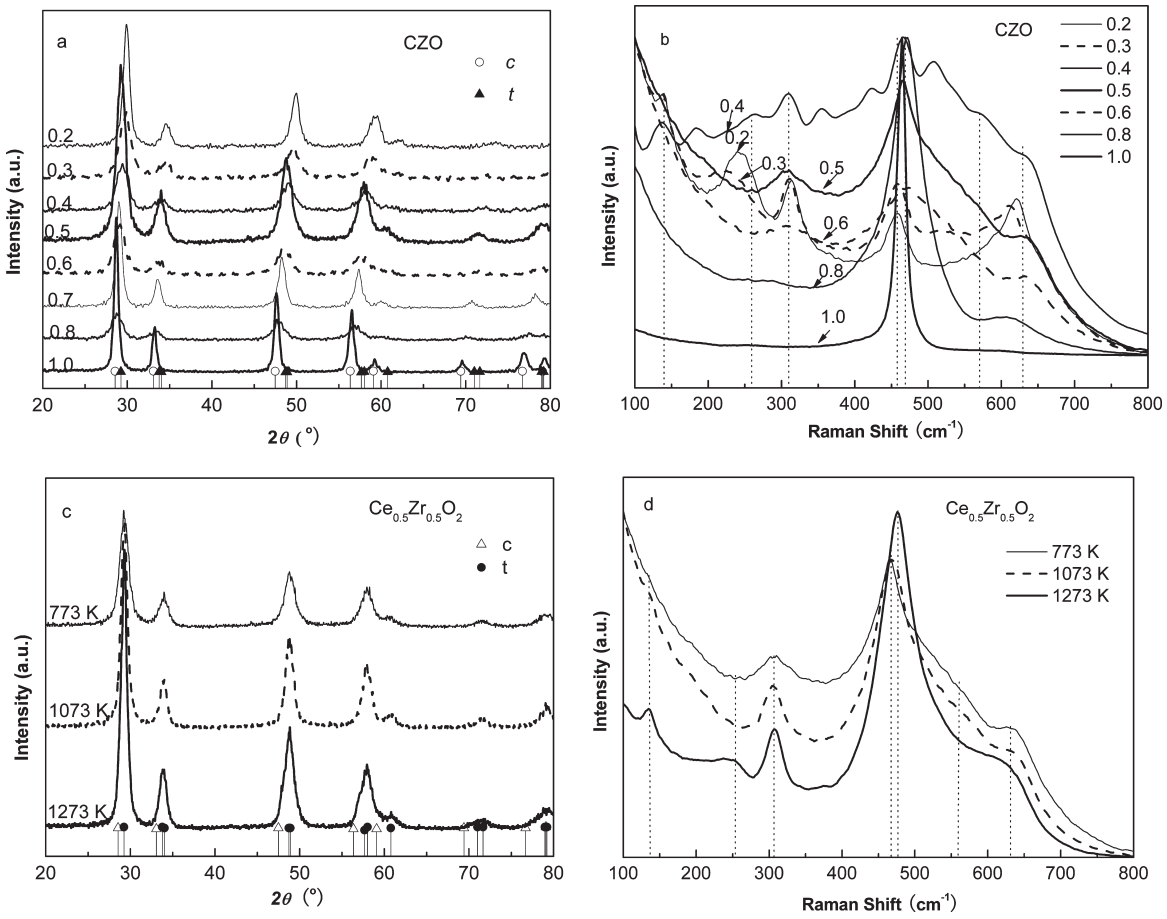

Figure 1. Wide-angle XRD patterns of CZO (a) and $Ce_{0.5}Zr_{0.5}O_2$ (c), and Raman shift of the CZO (b) and $Ce_{0.5}Zr_{0.5}O_2$ (d) samples.

Table 1. Crystal Sizes in the CZO Samples

x in $Ce_xZr_{1-x}O_2$	0.2	0.3	0.4	0.5	0.6	0.8	1.0
D/nm	24.9	19.8	7.8	19.5	8.9	8.2	15.3

center of CZO is located at 3.4 −3.8 nm, irrespective of the Ce/Zr molar ratio. However, they are bimodal mesoporous materials when x = 0.4, 0.5, 0.6; e.g., the pore center of $Ce_{0.5}Zr_{0.5}O_2$ calcined at 773 K is located at 3.8 and 22.3 nm. For the CZO samples, the BET surface areas and pore volumes gradually increased as the Ce/(Ce + Zr) ratio increased, reached a maximum at x = 0.6, then decreased at x = 1.0, except for some variation with x = 0.3 and 0.8. The BET surface area was directly related to the Ce/(Ce + Zr) ratio.

As shown in the SEM images of the $Ce_{0.5}Zr_{0.5}O_2$ samples (Figure 3), it was hard to observe any pores in the $Ce_{0.5}Zr_{0.5}O_2$ samples calcined at 773 K (Figure 3a). However, larger pores can be seen clearly in the $Ce_{0.5}Zr_{0.5}O_2$ samples calcined at 1073 K (Figure 3b). Well-defined PSD with diameters of about 0.9−1.5 μm appeared at 1273 K as shown in Figure 3c. The larger pores became more ordered with increasing calcination temperature.

The macropore size distribution, as measured by the mercury porosimetry, is shown in Figure 4. It clearly shows that the catalysts have bimodal meso/macropores with diameters of 2−47 nm and 1.4−3.4 μm at different calcination temperatures. These results are in agreement with the SEM results shown in Figure 3.

However, mercury porosimetry is only suitable for the determination of larger pores, thus the BJH method (Table 3) was used to measure the size distributions of the mesopores. As shown in Table 3, narrow peaks of the PSD were centered at 3.8 and 22.3 nm, 2.9 and 6.2 nm, and 2.4, 3.8, and 5.9 nm for the $Ce_{0.5}Zr_{0.5}O_2$ samples calcined at 773, 1173, and 1273 K, respectively. The pores had a bimodal distribution at 773 and 1173 K, and a trimodal distribution at 1273 K. However, the 923 and 1073 K samples had a single mode at 3.2 and 3.6 nm, respectively. These results indicated that $Ce_{0.5}Zr_{0.5}O_2$ can be prepared with narrower PSD by the present method, and the pore structure (bimodal or trimodal) and size can be controlled by varying the calcination temperature.

As the calcination temperature increased from 773 to 1073 K, the BET surface area of the $Ce_{0.5}Zr_{0.5}O_2$ samples decreased from 186.43 to 24.88 $m^2\ g^{-1}$, and then increased slightly as the calcination temperature increased from 1073 to 1273 K (Table 3). This may be related to the pore structure, i.e., there are multimodal mesoporous structure materials when the sample has been calcined at 773, 1173, and 1273 K. The BET surface area was larger when there were multiple pore structures.

H_2-TPR and CO_2 Adsorption. The TPR profiles of the fresh CZO samples are shown in Figure 5a. There are two peaks for all of the samples except those with x = 0.2, 0.8, and 1.0. Moreover, the peak at low temperature is shifted to lower temperature as the Ce content in the CZO sample increases. The peak at low temperature is believed to be reduction at the catalyst surface, while the peak at higher temperature is caused by the reduction

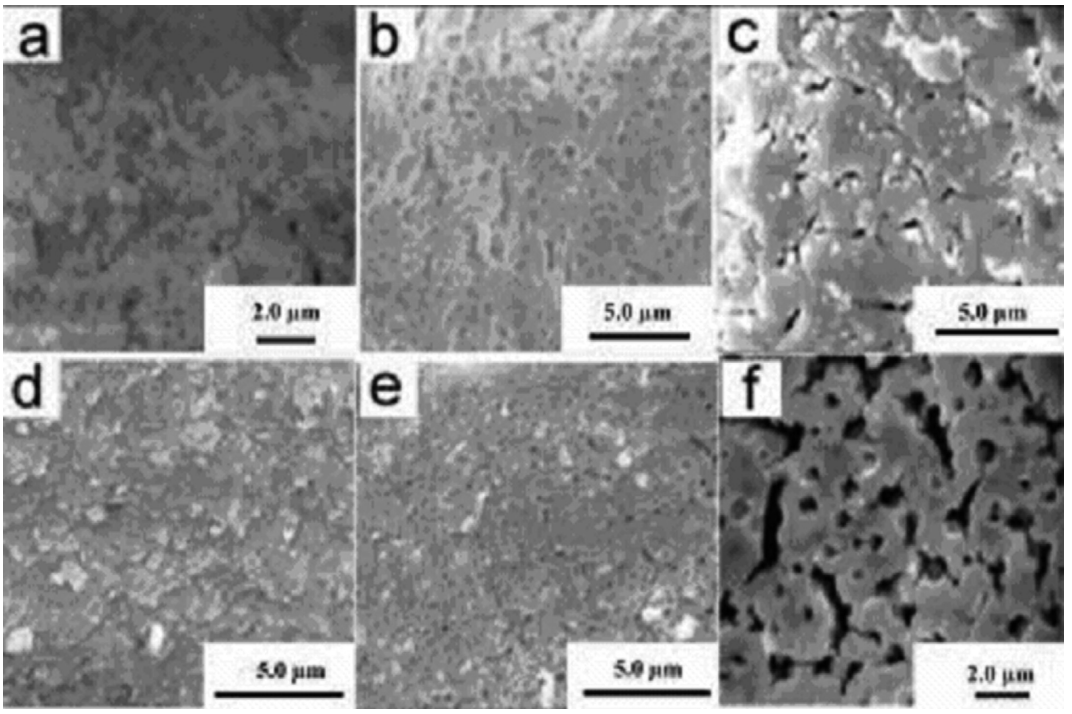

Figure 2. SEM micrographs of the CZO samples, with x of (a) = 0.2, (b) = 0.3, (c) = 0.4, (d) = 0.5, (e) = 0.6, and (f) = 0.8.

Table 2. Structural Properties of $Ce_xZr_{1-x}O_2$ Calcined at 773 K

Ce content (mol %)	BET surface area ($m^2\ g^{-1}$)	pore volume ($cm^3\ g^{-1}$)			BJH average pore width (nm)	pore center (nm)	CO_2 absorption ($cm^3\ g^{-1}$, STP)
		total	2−3 nm	>5 nm			
20	148.5	0.19	0.00	0.00	3.9	3.4	0. 50
30	136.2	0.32	0.00	0.00	5.6	3.4	0.44
40	163.3	0.29	0.09	0.00	4.5	2.2 and 3.7	0.31
50	186.4	0.77	0.03	0.71	15.4	3.8 and 22.3	0.87
60	204.6	0.79	0.16	0.63	7.2	3.3 and 4.8	2.74
80	179.3	0.48	0.10	0.38	4.0	3.6	1.47
100	193.4	0.57	0.00	0.74	8.0	3.5	1.50

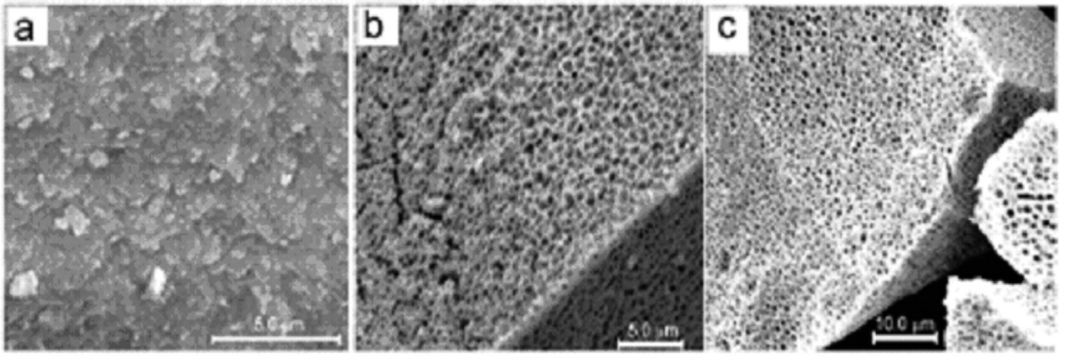

Figure 3. SEM micrographs of the $Ce_{0.5}Zr_{0.5}O_2$ samples calcined at (a) 773 K, (b) 1073 K, and (c) 1273 K.

of the bulk material.[21,32−36] As a consequence, we speculate that this shift in the low temperature region is a result of the high Ce content. As shown in the XRD results, the structure of CZO is dominated by the tetragonal phase at lower Ce content, while the structure of CZO is close to cubic phase with higher Ce content. This suggests the tetragonal phase is more difficult to reduce.

The TPR profiles of the fresh $Ce_{0.5}Zr_{0.5}O_2$ samples and the effects of subsequent reoxidation cycles are given in Figure 5b. There is only one peak for the $Ce_{0.5}Zr_{0.5}O_2$ sample calcined 1273

K, with a high reductive temperature, while all the other samples have two peaks. The reduction temperature in the low temperature region increases in temperature as the calcination temperature increases. This result corresponds to the structure of the materials, with the tetragonal phase being more difficult to reduce.

To probe the acid−base properties of the CZO and $Ce_{0.5}Zr_{0.5}O_2$ samples, the CO_2 adsorption of samples was investigated. As shown in Tables 2 and 3, for both the CZO and $Ce_{0.5}Zr_{0.5}O_2$ samples, the amount of CO_2 adsorption increased with the increase of the BET surface areas of samples. This indicates that there were more alkaline sites on the samples with higher BET surface areas. Moreover, the almost linear increase of the amount of CO_2 adsorbed with the increase of the BET surface area suggested the solid solutions have uniform surface acid−base properties. This also confirmed the formation of the $Ce_{0.5}Zr_{0.5}O_2$ solid solutions as determined by XRD patterns shown in Figure 1c, i.e., the homogeneously mixed Ce and Zr ions. The amount of catalytic active sites is related to the total amount of the reduction peak area. However, the catalytic activity is mainly related to the type and amount of active sites located on the catalyst surface. As shown in Figure 5b, there are at least two kinds of active sites on $Ce_{0.5}Zr_{0.5}O_2$ samples calcined at different temperatures.

Catalytic Activity over $Ce_xZr_{1-x}O_2$. Figure 6a shows the activity for the direct synthesis of DMC from CH_3OH and CO_2 over the CZO catalysts at 20 MPa and 373 K for 24 h. The selectivity to DMC increased when the ratio of Ce increased up to x = 0.4, then kept almost the same value. The methanol conversions (C_{CH_3OH}) increased with increase of the ratio Ce/Zr up to 0.5, then decreased. When the Ce/Zr molar ratio was about 1, the catalyst showed the highest catalytic performance without forming byproduct except H_2O. Thus the $Ce_{0.5}Zr_{0.5}O_2$ catalyst was selected for further studies.

Figure 6b shows the effect of the $Ce_{0.5}Zr_{0.5}O_2$ catalyst calcination temperatures on the methanol conversion. In all the experiments, ether and CO, which are the expected byproducts in DMC synthesis, were under the detection limit of the FID-GC analysis. The methanol conversion reached a maximum over the sample calcinated at 1273 K. However, the surface area of the $Ce_{0.5}Zr_{0.5}O_2$ decreased at higher calcination temperatures as indicated in Table 3. Thus, the amount of DMC formation was

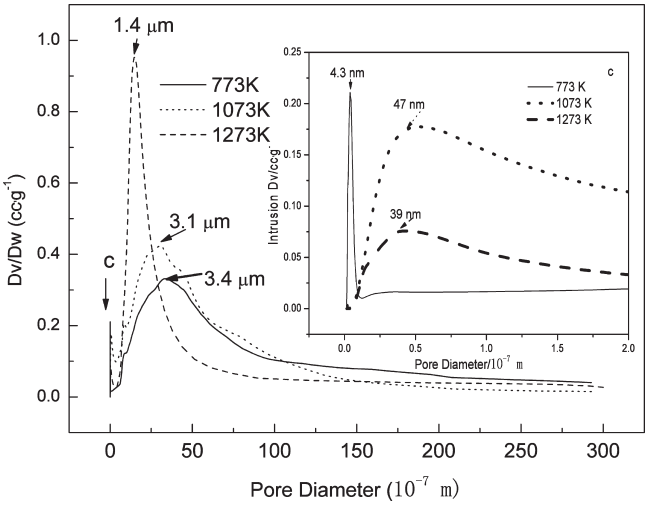

Figure 4. PSD of the $Ce_{0.5}Zr_{0.5}O_2$ samples calcined at different temperatures as determined by mercury porosimetry (the inset shows an enlargement of the PSDs of the small pores).

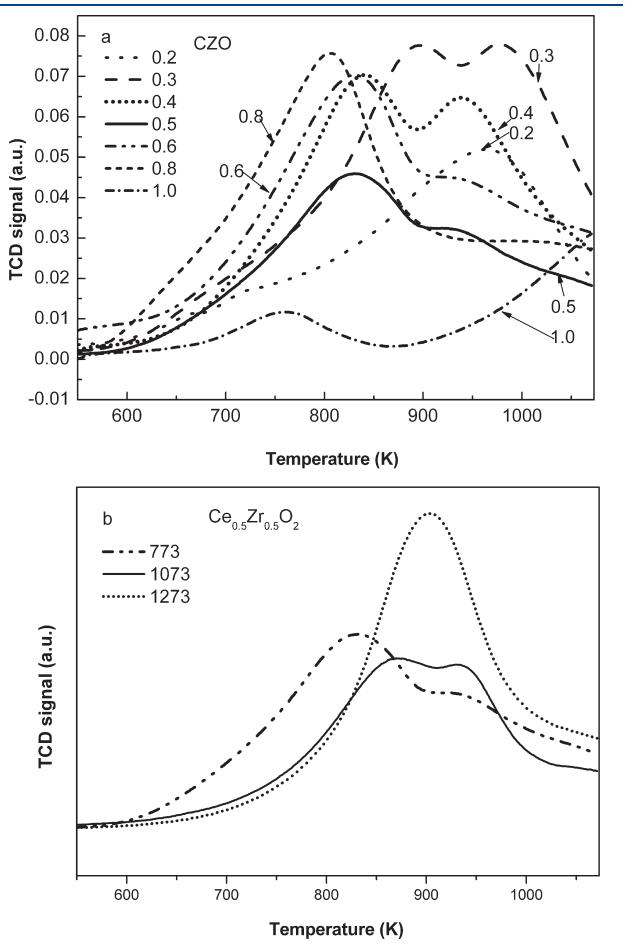

Figure 5. TPR profiles of the CZO samples (a) and the $Ce_{0.5}Zr_{0.5}O_2$ samples (b) calcined at different temperatures.

Table 3. Structural Properties of $Ce_{0.5}Zr_{0.5}O_2$ at Different Calcination Temperatures

calcination temperature (K)	BET surface area ($m^2\ g^{-1}$)	pore volume ($cm^3\ g^{-1}$)			BJH average pore width (nm)	pore center (nm)	CO_2 absorption ($cm^3\ g^{-1}$, STP)
		total	2−3 nm	>5 nm			
773	186.43	0.77	0.03	0.71	15.4	3.8 and 22.3	0.87
923	70.03	0.14	0.14	0.00	3.9	3.2	0.39
1073	24.88	0.06	0.06	0.00	6.5	3.6	0.30
1173	31.15	0.18	0.05	0.13	6.8	2.9 and 6.2	0.41
1273	36.82	0.18	0.00	0.17	18.9	2.4, 3.8, and 5.9	0.46

dx.doi.org/10.1021/ie102017j |Ind. Eng. Chem. Res. 2011, 50, 1981–1988

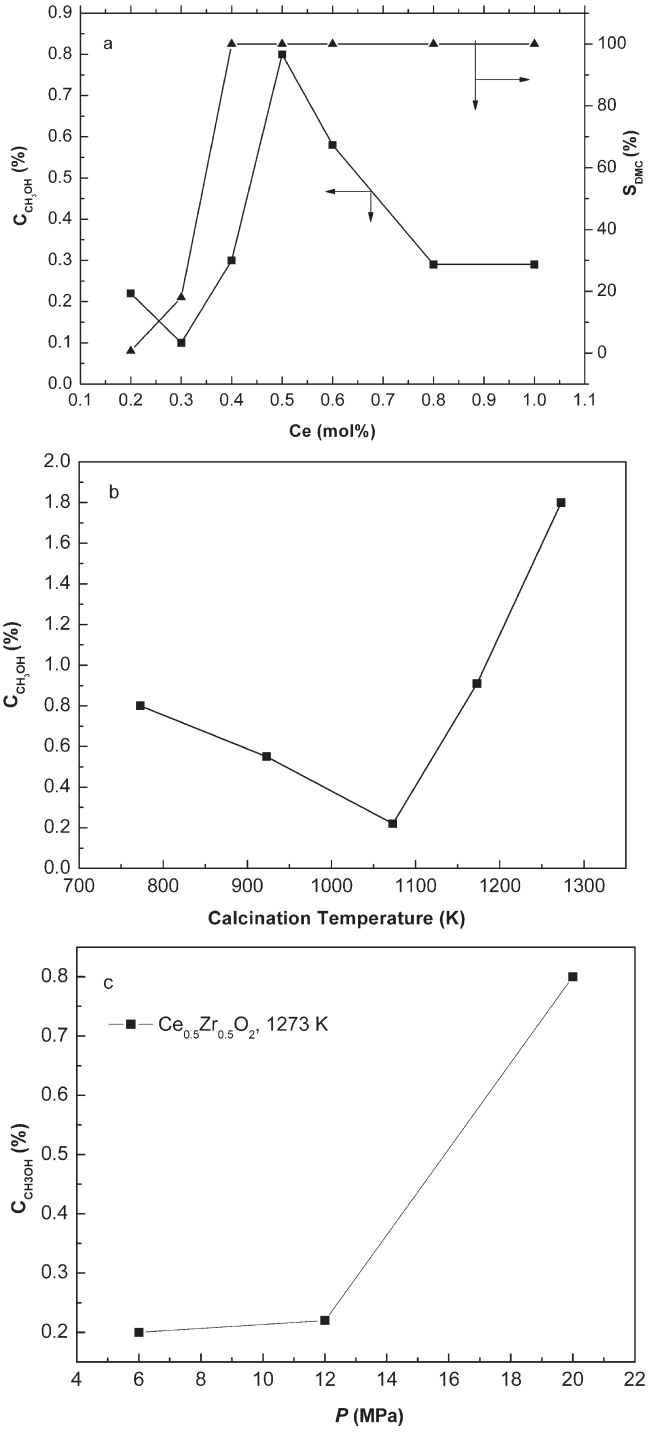

Figure 6. Dependence of the methanol conversion and the DMC selectivity on (a) Ce content in CZO catalysts, (b) the calcination temperatures over the $Ce_{0.5}Zr_{0.5}O_2$ catalysts (373 K, total pressure of 20 MPa, 24 h, and 0.5 g of catalyst), and (c) the reaction pressure (24 h, 373 K).

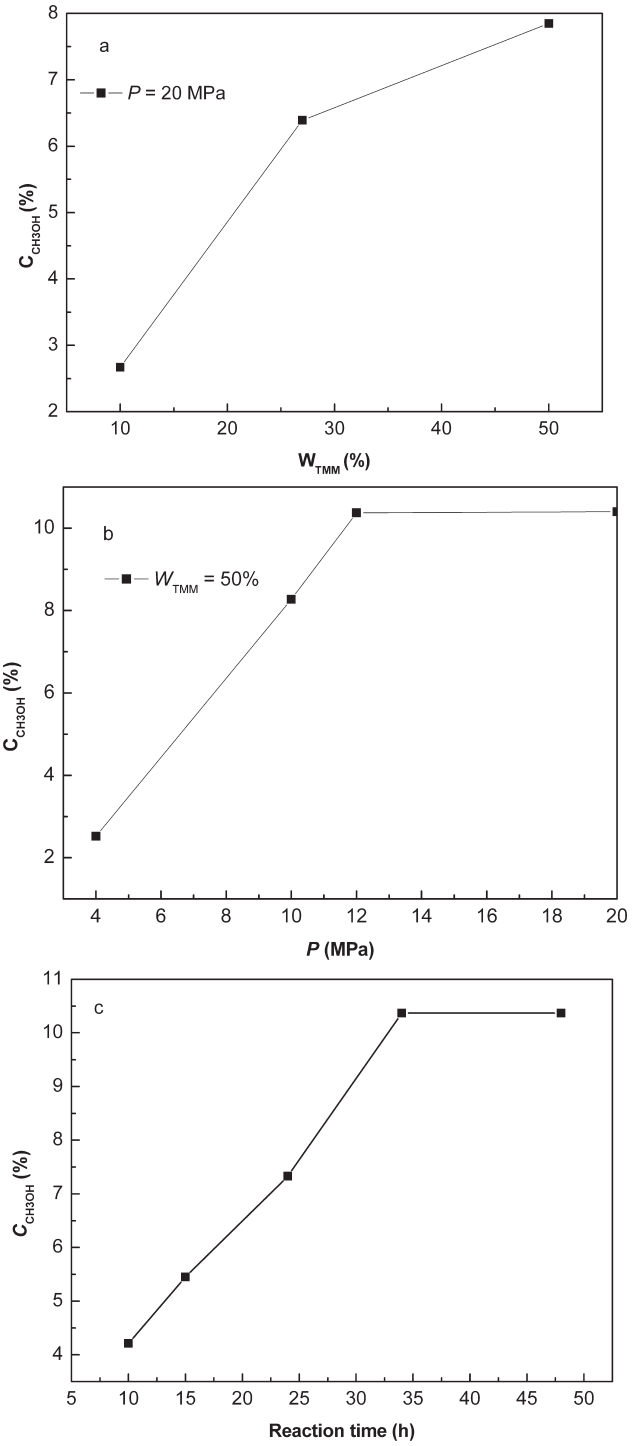

Figure 7. Dependence of methanol conversion on (a) the TMM ratio (20 MPa and 24 h), (b) the reaction pressure (50 wt % of TMM over 48 h), and (c) the reaction time (50 wt % of TMM at 12 MPa) over $Ce_{0.5}Zr_{0.5}O_2$ calcined at 1273 K.

not directly related to the surface area. Moreover, the methanol conversion was at a minimum over the $Ce_{0.5}Zr_{0.5}O_2$ samples calcined at 923 and 1073 K, which were the samples showing only a single pore size. Thus, the amount of DMC formation and the selectivity to DMC were strongly related to the catalyst structure, such as the surface acid−base property and the reduction degree, rather than to the surface area. The $Ce_{0.5}Zr_{0.5}O_2$ solid solution with a *t* phase structure and bimodal pore structure exhibited the highest DMC formation. Thus, the $Ce_{0.5}Zr_{0.5}O_2$ sample calcined at 1273 K was selected for further optimization.

Figure 6c shows the effect of the reaction pressure on the conversion of methanol. It is clear that the methanol conversion increased with increasing reaction pressure. It may be that the physical properties of CO_2, such as polarity and solubility, improved dramatically as the CO_2 became a supercritical fluid.[37,38]

Table 4. Effect of [EMIM]Br/$Ce_{0.5}Zr_{0.5}O_2$ Molar Ratio on DMC Formation[a]

[EMIM]Br/$Ce_{0.5}Zr_{0.5}O_2$ ratio	0	[EMIM]Br	1:1	1:2	1:3	1:4	1:10
C_{CH_3OH}/%	1.44	0.04	0.4	2.4	2	1.44	0.64

[a] 20 MPa, 24 h, CH_3OH 8 g, 0.5 g catalyst.

There are two phases for the mixture CO_2 and CH_3OH below the supercritical condition, while only one phase under the supercritical condition, which is favorite to the catalytic performance. The interactions between CO_2 and CH_3OH under supercritical fluids are under investigation.

However, the methanol conversion was still low, and was limited by the thermodynamics of this reaction. Thus an additive was used to remove the water produced from the reaction system, which promotes a shift in the equilibrium to the right. The addition of TMM (eq 2) was used to consume water at 373 K (Figure 7).

From Figure 7a, the methanol conversion increased as the amount of TMM increased, at the standard reaction conditions of 20 MPa and a duration of 24 h. The methanol conversion reached 7.85% which is much higher than the equilibrium conversion when 50 wt % TMM was introduced in the titled reaction. Again (Figure 7b), the methanol conversion increased with increasing reaction pressure to a maximum of 10.4% at 12 MPa, with 50 wt % TMM, over 48 h. These conditions were then used to investigate the optimum reaction time (Figure 7c), which showed the methanol conversion increased to a maximum at 34 h. This level of conversion is far above the equilibrium value. Aouissi et al.[39] reported that a highest conversion (7.6%) and highest DMC selectivity (86.5%) were obtained at the lowest temperature used (200 °C) over $Co_{1.5}PW_{12}O_{40}$ Keggin-type heteropolyanion, which is lower than the present results with a maximum methanol conversion of 10.4% and selectivity to DMC of 100%.

A blank test was studied under the same reaction conditions as that of the DMC synthesis for the reaction described in eq 3. Much less DMC was formed from TMM and CO_2, even though eq 3 is thermodynamically favorable. It was likely that the catalyst was not selectively favorable for the reaction in eq 3, but showed higher selectivity for the title reaction.

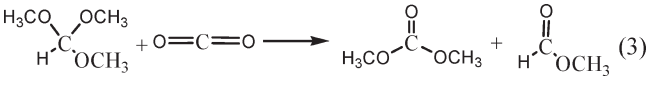

(3)

Catalytic Activity over [EMIM]Br/$Ce_{0.5}Zr_{0.5}O_2$. The $Ce_{0.5}Zr_{0.5}O_2$ catalyst loaded on [EMIM]Br ionic liquid showed promising catalytic activity for the title reaction as detailed in Table 4. The DMC productivity almost doubled when $Ce_{0.5}Zr_{0.5}O_2$ was loaded on [EMIM]Br with a [EMIM]Br to $Ce_{0.5}Zr_{0.5}O_2$ ratio of 1/3.

By examining the physical properties of the solid solutions of $Ce_xZr_{1-x}O_2$, the methanol conversion was related directly to Ce/Zr molar ratio, the crystal structure, and the pore structure. The Ce/Zr molar ratio was the key factor, with the $Ce_{0.5}Zr_{0.5}O_2$ solid solution the preferred ratio. For the $Ce_{0.5}Zr_{0.5}O_2$ solid solution, the crystal structure was an important factor, with the tetragonal phase giving the best DMC formation. In addition, the pore structure related the BET surface area and pore volume to the catalytic activity.

The acid−base properties of the solid solutions are clearly related to the BET surface area. The H-TPR was also related the structure of the solid solutions. These variations did not seem to be related to the formation of DMC. It seems that the low productivity is due to the equilibrium limitations of the reaction caused by the coproduced water.

The addition of TMM enhances the conversion of methanol. TMM readily reacted with H_2O under the reaction conditions. This made the equilibrium of the title reaction shift to the right, overcoming the thermodynamic limitations of the reaction. By examining the methanol conversion, 50 wt % of TMM gave the maximum conversion of 10.4% at 12 MPa over 34 h, far above the equilibrium value.

The [EMIM]Br/$Ce_{0.5}Zr_{0.5}O_2$ catalyst exhibited promising catalytic activity for the title reaction, which may provide a new process for the selective production of DMC starting from CO_2 and CH_3OH.

CONCLUSIONS

$Ce_xZr_{1-x}O_2$ solid solutions with different Ce/Zr molar ratios were synthesized via the citric acid sol−gel method. The crystal structures varied with the different molar ratios of the materials. The $Ce_{0.5}Zr_{0.5}O_2$ solid solution was similar to the tetragonal structure when the calcination temperature was 1273 K and the crystal size increased as the calcination temperature increased from 773 to 1273 K.

$Ce_{0.5}Zr_{0.5}O_2$ calcined at 1273 K was confirmed to have a bimodal pore structure with both meso and macropores, and showed higher catalytic performance for selective conversion of CH_3OH and CO_2 to DMC. The addition of TMM can overcome the thermodynamic limitations of this reaction by reacting with the coproduced H_2O, enhancing the conversion of methanol from 1.8% to 7.85%. When the amount of TMM reached 50 wt %, the methanol conversion reached a maximum of 10.4% at 12 MPa over 34 h, which is significantly above the equilibrium value.

The [EMIM]Br/$Ce_{0.5}Zr_{0.5}O_2$ catalyst exhibited higher catalytic activity than the $Ce_{0.5}Zr_{0.5}O_2$ catalyst for the production of DMC from CH_3OH and CO_2.

Further investigation into the surface structure and acid−base properties is necessary to elucidate the positive effect of high temperature calcination. In addition, the preparation of a catalyst with a larger surface area while maintaining the bimodal pore structure may dramatically increase the activity of DMC formation. Investigations into the surface structure and acid−base properties are in progress.

AUTHOR INFORMATION

Corresponding Author

*Tel.: +86 29 85303682. Fax: +86 29 85307774. E-mail: ztliu@snnu.edu.cn.

ACKNOWLEDGMENT

We gratefully acknowledge financial support from the National Natural Science Foundation of China (NSFC) (Grant 20976102). We thank the 973 Program of China (Program/Grant 2009CB226105) and the Natural Science Foundation of Education Department of Shaanxi Provincial Government (09JK844) for their support.

REFERENCES

(1) Selva, M.; Marques, C. A.; Tundo, P. Selective Mono-methylation of Arylacetonitriles and Methyl Arylacetates by Dimethyl Carbonate. *J. Chem. Soc., Perkin Trans.* **1994**, *1*, 1323.

(2) Bomben, A.; Marques, C. A.; Selva, M.; Tundo, P. A New Synthesis of 2-aryloxypropionic Acids Derivatives via Selective Mono-c-methylation of Methyl Aryloxyacetates and Aryloxyacetonitriles with Dimethyl Carbonate. *Tetrahedron* **1995**, *51*, 11573.

(3) Rivetti, F.; Romano, U.; Delledonne, D. In Anastas, P. T., Williamson, T. S., Eds. *Green Chemistry. Designing Chemistry for the Environment*; ACS Symposium Series No. 626; American Chemical Society: Washington, DC, 1996; p 70.

(4) Rivetti, F. In Anastas, P. T., Tundo, P., Eds.; *Green Chemistry: Challenging Pespectives*; Oxford University Press: Oxford, U.K., 2001.

(5) Pacheco, M. A.; Marshall, C. L. Review of Dimethyl Carbonate (DMC) Manufacture and Its Characteristics as a Fuel Additive. *Energy Fuels* **1997**, *11*, 2.

(6) Aresta, M.; Galatola, M. J. Life Cycle Analysis Applied to the Assessment of the Environmental Impact of Alternative Synthetic Processes. The Dimethylcarbonate Case: Part 1. *J. Clean. Prod.* **1999**, *7*, 181.

(7) Peppel, W. J. Preparation and Properties of the Alkylene Carbonates. *Ind. Eng. Chem.* **1958**, *50*, 767.

(8) Delledonne, D.; Rivetti, F.; Romano, U. Developments in the Production and Application of Dimethylcarbonate. *Appl. Catal. A: Gen.* **2001**, *221*, 241.

(9) Leino, E.; Mäki-Arvela, P.; Eta, V.; Murzin, D.; Yu.; Salmi, T.; Mikkola, J.-P. Conventional Synthesis Methods of Short-chain Dialkylcarbonates and Novel Production Technology via Direct Route from Alcohol and waste CO_2. *Appl. Catal. A: Gen.* **2010**, *383*, 1.

(10) Aresta, M.; Dibenedetto, A.; Nocito, F.; Angelini, A.; Gabriele, B.; Negri, S. D. Synthesis and Characterization of a Novel Polystyrene-tethered Niobium Methoxo Species. Its Application in the CO_2-based Carboxylation of Methanol to Afford Dimethyl Carbonate. *Appl. Catal. A: Gen.* **2010**, *387*, 113.

(11) Almusaiteer, K. Synthesis of Dimethyl Carbonate (DMC) from Methanol and CO_2 over Rh-supported Catalysts. *Catal. Commun.* **2009**, *10*, 1127.

(12) Omae, I. Aspects of Carbon Dioxide Utilization. *Catal. Today* **2006**, *115*, 33.

(13) Yin, X. L.; Moss, J. R. Recent Developments in the Activation of Carbon Dioxide by Metal Complexes. *Coord. Chem. Rev.* **1999**, *181*, 27.

(14) Kizlink, J. Synthesis of Dimethyl Carbonate from Carbon Dioxide and Methanol in the Presence of Organotin Compounds. *Collect. Czech. Chem. Commun.* **1993**, *58*, 1399.

(15) Fang, S.; Fujimoto, K. Direct Synthesis of Dimethyl Carbonate from Carbon Dioxide and Methanol Catalyzed by Base. *Appl. Catal. A: Gen.* **1996**, *142*, L1.

(16) Tomishige, K.; Kunimori, K. Catalytic and Direct Synthesis of Dimethyl Carbonate Starting from Carbon Dioxide using CeO_2-ZrO_2 Solid Solution Heterogeneous Catalyst: Effect of H_2O Removal from the Reaction System. *Appl. Catal. A: Gen.* **2002**, *237*, 103.

(17) Jiang, C.; Guo, Y.; Wang, C.; Hu, C.; Wu, Y.; Wang, E. Synthesis of Dimethyl Carbonate from Methanol and Carbon Dioxide in the Presence of Polyoxometalates under Mild Conditions. *Appl. Catal. A: Gen.* **2003**, *256*, 203.

(18) Wu, X. L.; Xiao, M.; Meng, Y. Z.; Lu, Y. X. Direct Synthesis of Dimethyl Carbonate on H_3PO_4 Modified V_2O_5. *J. Mol. Catal. A: Chem.* **2005**, *238*, 158.

(19) Tomishige, K.; Sakaihori, T.; Ikeda, Y.; Fujimoto, K. A Novel Method of Direct Synthesis of Dimethyl Carbonate from Methanol and Carbon Dioxide Catalyzed by Zirconia. *Catal. Lett.* **1999**, *58*, 225.

(20) Tomishige, K.; Furusawa, Y.; Ikeda, Y.; Asadullah, M.; Fujimoto, K. CeO_2−ZrO_2 Solid Solution Catalyst for Selective Synthesis of Dimethyl Carbonate from Methanol and Carbon Dioxide. *Catal. Lett.* **2001**, *76*, 71.

(21) Yoshida, Y.; Arai, Y.; Kado, S.; Kunimori, K.; Tomishige, K. Direct Synthesis of Organic Carbonates from the Reaction of CO_2 with Methanol and Ethanol over CeO_2 Catalysts. *Catal. Today* **2006**, *115*, 95.

(22) Cutrufello, M. G.; Ferino, I.; Solinas, V.; Primavera, A.; Trovarelli, A.; Auroux, A.; Picciau, C. Acid−base Properties and Catalytic Activity of Nanophase Ceria−zirconia Catalysts for 4-methylpentan-2-ol Dehydration. *Phys. Chem. Chem. Phys.* **1999**, *1*, 3369.

(23) Tomishige, K.; Furusawa, Y.; Ikeda, Y.; Asadullah, M.; Fujimoto, K. CeO_2-ZrO_2 Solid Solution Catalyst for Selective Synthesis of Dimethyl Carbonate from Methanol and Carbon Dioxide. *Catal. Lett.* **2001**, *76*, 71.

(24) Ma, Z.-B. Progress in the Synthesis and Characterization of Carbon Nitride Crystals. *New Carbon Mater.* **2006**, *21*, 277.

(25) Choi, J.-C.; Sakakura, T.; Sako, T. Reaction of Dialkyltin Methoxide with Carbon Dioxide Relevant to the Mechanism of Catalytic Carbonate Synthesis. *J. Am. Chem. Soc.* **1999**, *121*, 3793.

(26) Choi, J.-C.; He, L. N.; Yasuda, H.; Sakakura, T. Selective and High Yield Synthesis of Dimethyl Carbonate Directly from Carbon Dioxide and Methanol. *Green Chem.* **2002**, *4*, 230.

(27) Hou, Z. S.; Han, B. X.; Liu, Z. M.; Jiang, T.; Yang, G. Y. Synthesis of Dimethyl Carbonate Using CO_2 and Methanol: Enhancing the Conversion by Controlling the Phase Behavior. *Green Chem.* **2002**, *4*, 467.

(28) Chen, X. Z.; Hu, C. W.; Su, J. H.; Yu, T.; Gao, Z. M. One-Pot Synthesis of Dimethyl Carbonate Catalyzed by $[BMIM]BF_4/CH_3ONa$. *Chin. J. Catal.* **2006**, *27*, 485.

(29) López, E. F.; Escribano, V. S.; Panizza, M.; Carnasciali, M. M.; Busca, G. Vibrational and Electronic Spectroscopic Properties of Zirconia Powders. *J. Mater. Chem.* **2001**, *11*, 1891.

(30) McBride, J. R.; Hass, K. C.; Poindexter, B. D.; Weber, W. H. Raman and X-ray Studies of $Ce_{1-x}RE_xO_{2-y}$ Where RE=La, Pr, Nd, Eu, Gd and Tb. *J. Appl. Phys.* **1994**, *76*, 2435.

(31) Yuan, Q.; Liu, Q.; Song, W. G.; Feng, W.; Pu, W. L.; Sun, L. D.; Zhang, Y. W.; Yan, C. H. Ordered Mesoporous $Ce_{1-x}Zr_xO_2$ Solid Solutions with Crystalline Walls. *J. Am. Chem. Soc.* **2007**, *129*, 6698.

(32) Otsuka, K.; Wang, Y.; Nakamura, M. Direct conversion of methane to synthesis gas through gas-solid reaction using CeO_2-ZrO_2 solid solution at moderate temperature. *Appl. Catal. A: Gen.* **1999**, *183*, 317.

(33) Trovarelli, A.; Zamar, F.; Llorca, J.; Leitenburg, C. D.; Dolcetti, G.; Kiss, J. T. Nanophase Fluorite-Structured CeO_2−ZrO_2 Catalysts Prepared by High-Energy Mechanical Milling. *J. Catal.* **1997**, *169*, 490.

(34) Yao, H. C.; Yao, Y. F. Y. Ceria in Automotive Exhaust Catalysts: I. Oxygen storage. *J. Catal.* **1984**, *86*, 254.

(35) Kašpar, J.; Fornasiero, P.; Graziani, M. Use of CeO_2-based Oxides in the Three-way Catalysis. *Catal. Today* **1999**, *50*, 285.

(36) Fally, F.; Perrichon, V.; Vidal, H.; Kaspar, J.; Blanco, G.; Pintado, J. M.; Bernal, S.; Colon, G.; Daturi, M.; Lavalley, J. C. Modification of the Oxygen Storage Capacity of CeO_2−ZrO_2 Mixed Oxides after Redox Cycling Aging. *Catal. Today* **2000**, *59*, 373.

(37) Sakakura, T.; Choi, J. C.; Saito, Y.; Masuda, T.; Sako, T.; Oriyama, T. Metal-Catalyzed Dimethyl Carbonate Synthesis from Carbon Dioxide and Acetals. *J. Org. Chem.* **1999**, *64*, 4506.

(38) Noyori, R. Supercritical Fluids: Introduction. *Chem. Rev.* **1999**, *99*, 353.

(39) Aouissi, A.; Al-Othman, Z. A.; Al-Amro, A. Gas-Phase Synthesis of Dimethyl Carbonate from Methanol and Carbon Dioxide Over $Co_{1.5}PW_{12}O_{40}$ Keggin-Type Heteropolyanion. *Int. J. Mol. Sci.* **2010**, *11*, 1343.